Int. J. Heat Mass Transfer. Vol. 33, No. 6, pp. 1183–1192, 1990
Printed in Great Britain

0017-9310/90 $3.00+0.00

Study of laminar heat transfer over a sinusoidal-shaped rotating disk

G. LE PALEC, P. NARDIN and D. RONDOT
G.R.G.T., Institut Universitaire de Technologie, Rue Engel Gros, B.P. 527, 90016 Belfort Cedex, France

(*Received* 23 *February* 1989 *and in final form* 10 *August* 1989)

Abstract—A theoretical and experimental investigation of laminar convective heat transfer over a sinusoidal-shaped rotating disk with a constant wall heat flux condition is presented. The theory is based upon the boundary-layer approach. The results show the effects of roughness on the local and average Nusselt numbers. Theoretical wall temperatures are obtained from a simple thermal balance and compared with the experimental ones measured by means of an infra-red thermography technique for the case of air ($Pr = 0.7$).

1. INTRODUCTION

IN THE BULK of theoretical studies about convective heat transfer, the calculation procedure of the local and average Nusselt numbers is facilitated by the assumption that the exchange surfaces are smooth. However, from an engineering point of view, the surfaces are rough and the wall roughness acts on the heat transfer coefficient. This phenomenon has been the subject of several experimental works because of its applications in many industrial processes such as heat exchangers, active sites in boiling processes, etc. [1–5]. All these studies treat laminar or turbulent flows over plates and duct flows.

From a theoretical standpoint, only a few studies have been reported in the literature and this is probably due to the difficulties encountered in describing the geometry of rough profiles. However, they can be modelled by a periodic distribution of the surface irregularities. In this way, the special case of sinusoidal-shaped areas is interesting to study and a number of papers about laminar heat transfer over sinusoidal plates for both forced [6, 7] and free [8] convection have been presented recently. On the other hand and to the best knowledge of the authors, the case of rough rotating bodies of revolution has not been investigated: this is the subject of this paper in which a theoretical and experimental analysis of laminar heat transfer over a rotating rough disk is presented. The roughness is modelled with sinusoids which are concentric with respect to the axis of rotation and the theory is limited to the case of small amplitude/wavelength ratio ($a_0/\lambda \leqslant 0.2$). The results are compared with those of the well-known isothermal flat disk problem [9–12] which appears as a limiting case of the present study. This theory has been validated with measurements of the wall temperatures for the case of air, using an infra-red thermography technique.

2. THEORETICAL ANALYSIS

Consider (Fig. 1) a sinusoidal-shaped disk with radius L which rotates with angular velocity ω in a newtonian fluid at rest. The physical properties of the fluid are constant and its temperature far from the wall is T_∞. We choose an orthogonal curvilinear coordinate system with x measuring the distance from the axis, along the surface curvature, y and θ being, respectively, the normal distance from the wall and the azimuthal direction. From laminar boundary-layer theory, the governing equations for axisymmetric flow are:

continuity

$$\frac{\partial V_x}{\partial x} + \frac{\partial V_y}{\partial y} + \frac{V_x}{r}\frac{\mathrm{d}r}{\mathrm{d}x} = 0; \tag{1}$$

momentum

$$V_x\frac{\partial V_x}{\partial x} + V_y\frac{\partial V_x}{\partial y} - \frac{V_\theta^2}{r}\frac{\mathrm{d}r}{\mathrm{d}x} = \nu\frac{\partial^2 V_x}{\partial y^2} \tag{2}$$

$$V_x\frac{\partial V_\theta}{\partial x} + V_y\frac{\partial V_\theta}{\partial y} + \frac{V_x V_\theta}{r}\frac{\mathrm{d}r}{\mathrm{d}x} = \nu\frac{\partial^2 V_\theta}{\partial y^2}; \tag{3}$$

energy

$$V_x\frac{\partial T}{\partial x} + V_y\frac{\partial T}{\partial y} = a\frac{\partial^2 T}{\partial y^2} \tag{4}$$

where V_x, V_y and V_θ are the velocity components corresponding to the x, y and θ directions; r is the normal distance from the axis of rotation; a and ν are, respectively, the thermal diffusivity and the kinematic viscosity of the fluid, the temperature of which is T in the boundary layer. For a flat rotating disk, the boundary-layer thickness δ is approximated as $\delta \simeq (\nu/\omega)^{1/2}$. In this study, the wavelength λ is the characteristic length so that equations are valid only if $(\lambda^2\omega/\nu)^{1/2} \gg 1$. The boundary conditions associated

NOMENCLATURE

a thermal diffusivity of the fluid [$m^2 s^{-1}$]
a_0 amplitude of the sinusoidal profile [m]
C_P specific heat of air [$J kg^{-1} s^{-1}$]
$f(\varepsilon,\eta)$, $g(\varepsilon,\eta)$ dimensionless stream functions
h local convective heat transfer coefficient [$W m^{-2} K^{-1}$]
g_0 gravitational acceleration [$m s^{-2}$]
Gr Grashof number, $\beta_T g_0 (T_w - T_\infty)\lambda^3/\nu^2$
k thermal conductivity of the fluid [$W m^{-1} K^{-1}$]
L radius of the disk [m]
Nu local Nusselt number, $h\lambda/k$
$\overline{Nu}$ average Nusselt number related to the real surface of the disk
$\overline{Nu_P}$ average Nusselt number related to the surface of the smooth disk, πL^2
Pr Prandtl number, $\mu C_P/k$
Q incident heat flux [$W m^{-2}$]
q wall heat balance [$W m^{-2}$]
r radial distance from the axis [m]
R dimensionless radial distance from the axis
Re_ω Reynolds number, $\lambda^2\omega/\nu$
Ri Richardson number, Gr/Re_ω^2
S real surface area of the disk [m^2]
T temperature of the fluid in the boundary layer [K]
T_{max} average maximum temperature of the disk [K]
T_∞ temperature of the fluid far from the wall [K]
T_w wall temperature [K]
V_x, V_y, V_z velocity components [$m s^{-1}$]
x, y, z orthogonal curvilinear coordinates (Fig. 1) [m].

Greek symbols
α_r, ε_r absorptivity and emissivity of the surface
β angle defined in Fig. 1 [rad]
β_T coefficient of thermal expansion [K^{-1}]
ε, η dimensionless coordinates
θ_T dimensionless temperature
θ_{T_0} wall dimensionless temperature
λ wavelength of the sinusoidal profile [m]
μ dynamic viscosity of the fluid [$kg m^{-1} s^{-1}$]
ν kinematic viscosity of the fluid [$m^2 s^{-1}$]
σ Stefan–Boltzmann constant [$W m^{-2} K^{-4}$]
$\phi(x, y)$, $\psi(x, y)$ stream functions [$m^2 s^{-1}$]
ω angular velocity of the disk [$rad s^{-1}$].

with the differential system (1)–(4) are written by introducing the wall heat flux q:

$$\left.\begin{aligned} &\text{for } y = 0: \quad V_x = V_y = V_\theta - r\omega = 0 \\ &\qquad\qquad -k\frac{\partial T}{\partial y} = q \\ &\text{for } y \to \infty: \quad V_x \to 0, \quad V_\theta \to 0, \quad T \to T_\infty \end{aligned}\right\}. \tag{5}$$

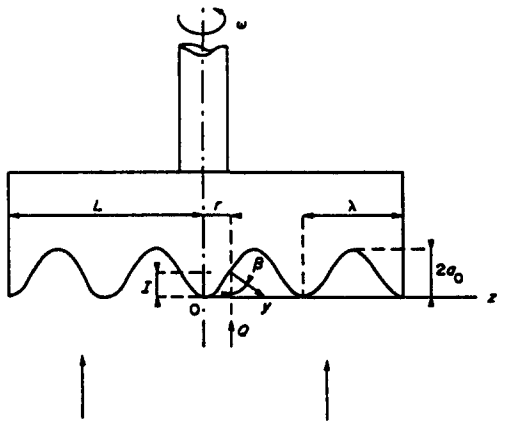

FIG. 1. Problem statement and definition of the coordinates and definition of the parameters used for the calculation of the curvilinear abscissa.

Equations (1)–(4) subjected to the boundary conditions (5) are solved by introducing the following non-dimensional coordinate system:

$$\left.\begin{aligned} \varepsilon &= \frac{x}{\lambda} \\ \eta &= \left(\frac{\omega R}{\nu\varepsilon}\right)^{1/2} y \end{aligned}\right\} \tag{6}$$

where R is the ratio r/λ. We also define the dimensionless stream functions $f(\varepsilon,\eta)$ and $g(\varepsilon,\eta)$ as

$$\left.\begin{aligned} f(\varepsilon,\eta) &= \sqrt{\left(\frac{\omega R}{\nu\varepsilon}\right)}\frac{\psi(x,y)}{\omega r} \\ g(\varepsilon,\eta) &= \sqrt{\left(\frac{\omega R}{\nu\varepsilon}\right)}\frac{\phi(x,y)}{\omega r} \end{aligned}\right\} \tag{7}$$

where $\psi(x, y)$ and $\phi(x, y)$ are the stream functions which are related to the velocity components by

$$\left.\begin{aligned} V_x &= \frac{1}{r}\frac{\partial\psi(x,y)r}{\partial y} \\ V_y &= -\frac{1}{r}\frac{\partial\psi(x,y)r}{\partial x} \\ V_\theta &= \frac{\partial\phi(x,y)}{\partial y} \end{aligned}\right\}. \tag{8}$$

Finally, we introduce a dimensionless temperature $\theta_T(\varepsilon, \eta)$

$$\theta_T(\varepsilon,\eta) = \frac{(T-T_\infty)k}{q}\left(\frac{\omega R}{\nu\varepsilon}\right)^{1/2} \tag{9}$$

with k being the thermal conductivity of the fluid. It can be shown that substituting relations (8) and (9) into equations (1)–(4) and boundary conditions (5) and using definitions (6) and (7) leads to the following differential system:

$$f''' - \frac{\varepsilon}{R}\frac{\mathrm{d}R}{\mathrm{d}\varepsilon}(f'^2 - g'^2) + \left(\frac{1}{2} + \frac{3}{2}\frac{\varepsilon}{R}\frac{\mathrm{d}R}{\mathrm{d}\varepsilon}\right)ff'' = \varepsilon\left(f'\frac{\partial f'}{\partial\varepsilon} - f''\frac{\partial f}{\partial\varepsilon}\right) \tag{10}$$

$$g''' + \left(\frac{1}{2} + \frac{3}{2}\frac{\varepsilon}{R}\frac{\mathrm{d}R}{\mathrm{d}\varepsilon}\right)g''f - \frac{2\varepsilon}{R}\frac{\mathrm{d}R}{\mathrm{d}\varepsilon}f'g' = \varepsilon\left(f'\frac{\partial g'}{\partial\varepsilon} - g''\frac{\partial f}{\partial\varepsilon}\right) \tag{11}$$

$$Pr^{-1}\theta_T'' + \left(\frac{1}{2} + \frac{3}{2}\frac{\varepsilon}{R}\frac{\mathrm{d}R}{\mathrm{d}\varepsilon}\right)f\theta_T' = \varepsilon\left(f'\frac{\partial\theta_T}{\partial\varepsilon} - \theta_T'\frac{\partial f}{\partial\varepsilon}\right) \tag{12}$$

with

$$\begin{aligned} &\text{for } \eta = 0: \quad f = g = f' = 0, \quad g' = 1, \quad \theta_T' = -1 \\ &\text{for } \eta \to \infty: \quad f' \to 0, \quad g' \to 0, \quad \theta_T \to 0. \end{aligned} \tag{13}$$

In the above equations Pr is the Prandtl number and the 'primes' denote differentiation with respect to η. The boundary conditions with respect to ε are obtained by solving equations (10)–(13) at the axis where all derivatives $\partial/\partial\varepsilon$ vanish because of the symmetry of velocity and temperature profiles with respect to the axis of rotation. With γ denoting the limiting value of $\varepsilon/R \cdot \mathrm{d}R/\mathrm{d}\varepsilon$ as $\varepsilon \to 0$, these conditions are:

for $\varepsilon = 0$

$$\left.\begin{aligned} &f''' - \gamma(f'^2 - g'^2) + ff''\left(\frac{1}{2} + \frac{3}{2}\gamma\right) = 0 \\ &g''' + \left(\frac{1}{2} + \frac{3}{2}\gamma\right)g''f - 2\gamma g'f' = 0 \\ &Pr^{-1}\theta_T'' + \left(\frac{1}{2} + \frac{3}{2}\gamma\right)f\theta_T' = 0 \end{aligned}\right\} \tag{14}$$

subjected to the boundary conditions (13).

2.1. *Calculation of the curvilinear abscissa x*

Consider the studied profile drawn in Fig. 1 with 1 being the normal distance from a point of the surface to the axis Oz. As explained above, x is the curvilinear distance and r is the radial distance from the axis of rotation ($r \equiv z$). We have

$$l = a_0\left[1 - \cos\frac{2\pi z}{\lambda}\right] = 2a_0\sin^2\frac{\pi z}{\lambda} \tag{15}$$

which gives

$$\mathrm{d}x = \sqrt{\left(1 - \frac{4a_0^2\pi^2}{\lambda^2}\sin^2\frac{2\pi z}{\lambda}\right)}\,\mathrm{d}z. \tag{16}$$

The distance x can thus be expressed as an elliptic integral of the second type [13]

$$x = K\int_0^z \sqrt{\left(1 - K'\sin^2\left(\frac{2\pi z}{\lambda} + \frac{\pi}{2}\right)\right)}\,\mathrm{d}z \tag{17}$$

with

$$\left.\begin{aligned} K &= \sqrt{\left(1 + \frac{4a_0^2\pi^2}{\lambda^2}\right)} \\ K' &= \frac{4a_0^2\pi^2}{\lambda^2 K} \end{aligned}\right\}. \tag{18}$$

By setting

$$Y = \frac{2\pi z}{\lambda} + \frac{\pi}{2}$$

we find

$$x = \frac{K\lambda}{2\pi}\int_{\pi/2}^{Y}\sqrt{(1 - K'\sin^2 Y)}\,\mathrm{d}Y. \tag{19}$$

From equations (16) and (19) it is now easy to calculate numerically ε and $\mathrm{d}R/\mathrm{d}\varepsilon$, which is identical to $\mathrm{d}z/\mathrm{d}x$.

2.2. *Calculation of the Nusselt number*

The non-dimensional wall temperature θ is one of the physically interesting functions because it is related to the local Nusselt number, Nu, which is defined in this study as

$$Nu = \frac{h\lambda}{k} \tag{20}$$

where h is the local heat transfer coefficient which can be expressed from the wall heat flux q as

$$h = \frac{q}{T_w - T_\infty} \tag{21}$$

T_w being the wall temperature. From equations (5), (6) and (9), we obtain

$$Nu\,Re_\omega^{-1/2} = \left(\frac{R}{\varepsilon}\right)^{1/2}\frac{1}{\theta_{T_0}}. \tag{22}$$

Re_ω is the Reynolds number for which the definition is

$$Re_\omega = \frac{\omega\lambda^2}{\nu}. \tag{23}$$

Integrating equation (22) yields the average Nusselt number $\overline{Nu}$

$$\overline{Nu}\, Re_\omega^{-1/2} = \frac{1}{S}\int_S Nu\, Re_\omega^{-1/2}\, dS \qquad (24)$$

where S is the area of the disk. In order to quantify the effect of roughness on heat transfer, it is also convenient to introduce the area (πL^2) as a reference. The corresponding average Nusselt number is

$$\overline{Nu_P} = \overline{Nu}\frac{S}{\pi L^2}. \qquad (25)$$

For a smooth disk, it is clear that $\overline{Nu_P}$ becomes identical to $\overline{Nu}$.

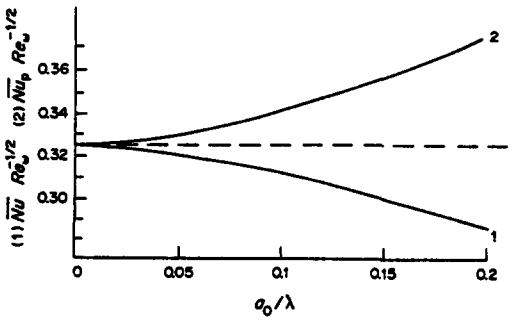

FIG. 3. Variation of the average Nusselt numbers $\overline{Nu}$ (curve 1) and $\overline{Nu_P}$ (curve 2) vs the amplitude/wavelength ratio. $Pr = 0.7$, $L = 0.02$ m, $\lambda = 0.01$ m.

3. THEORETICAL RESULTS

Equations (10)–(12) and boundary conditions (13) have been discretized with a simple implicit finite difference scheme, similar to that used by Keller and Cebeci [14, 15]. For boundary-layer problems, this procedure is much faster than most other numerical methods and it enables us to compute very close to the point of flow separation. This last point is one of the disadvantages of classical methods such as Görtler expansions, see for example ref. [16]. The resulting non-linear system of equations has been solved by the Newton method with a block tridiagonal factorization technique [17].

The variations of the local Nusselt number depend on the amplitude/wavelength ratio a_0/λ. This is shown in Fig. 2 where the non-dimensional parameter $Nu\, Re_\omega^{-1/2}$ has been plotted against the radial distance from the axis of rotation for several values of a_0/λ (0, 1/16, 1/8 and 1/5) and for $Pr = 0.7$ (air). We first note that the thermal profile is a periodic function with a double periodicity as compared to that of the geometrical profile. It should be emphasized that these results were obtained by specifying a uniform wall heat flux, so that the radial variation of wall temperature together with the shape of the disk affect the local Nusselt number: the variation of wall temperature has a significant effect on the heat transfer from a flat rotating disk [10–12].

The double periodicity results from the change in the sign of $d^2R/d\varepsilon^2$ at the points $n\lambda/4$ (n is an integer): this change affects the value of the wall velocity gradients with an accompanying effect on the local heat transfer coefficient. However, the position of the maximum and minimum values departs from the points $n\lambda/4$ because the centrifugal forces influence the hydrodynamic and thermal boundary-layer thicknesses. We also note a decrease in the amplitudes of the profiles as the distance from the axis of rotation becomes greater. The maximum value of the local Nusselt number is observed at the axis where the thickness of the boundary layer, δ, is minimum, because of the curvature of the geometrical profile: the variation of δ as ε increases can be seen from equation (6), which shows that δ is proportional to $(\nu/\omega)^{1/2}(\varepsilon/R)^{1/2}$. For a flat rotating disk, ε is identical to R so that δ is uniform and proportional to $(\nu/\omega)^{1/2}$. For the rough disk, δ is proportional to $(\nu/\omega)^{1/2}$ only at $\varepsilon = 0$ because ε/R is then equal to 1. For $\varepsilon > 0$, δ increases with increasing values of $(\varepsilon/R)^{1/2}$. Finally, it should be noted that no secondary flow due to the concave surface occurs, which is probably the consequence of the assumption that $a_0/\lambda \ll 1$.

Figure 3 shows the variation of the average Nusselt number $\overline{Nu}\, Re_\omega^{-1/2}$ as a function of the ratio a_0/λ (curve 1). It is observed that $\overline{Nu}$ decreases as a_0/λ increases. However, as explained above, a rough surface must be defined with the area of the smooth disk as a reference. We then observe (curve 2) that the corresponding values of the average Nusselt number,

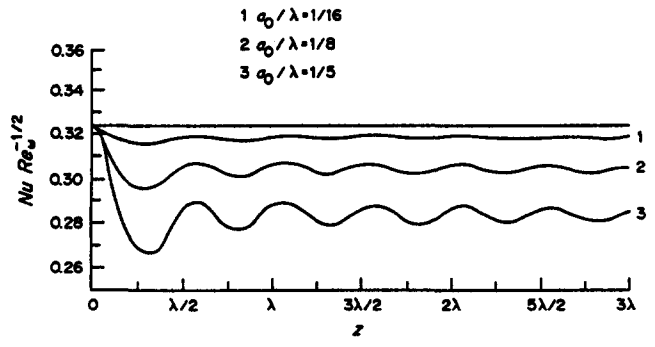

FIG. 2. Variation of the local Nusselt number vs the normal distance from the axis of rotation for several values of amplitude/wavelength ratio. $Pr = 0.7$, $L = 0.03$ m.

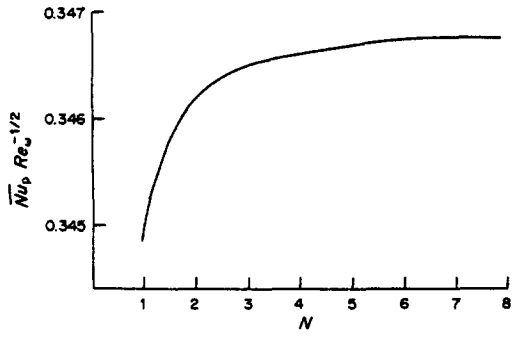

FIG. 4. Variation of the average Nusselt number $\overline{Nu_P}$ vs the number of sinusoids encountered on the disk area. $Pr = 0.7$, $a_0/\lambda = 0.125$, $L = 0.02$ m, $\lambda = 0.01$ m.

$\overline{Nu_P}$, increase as the ratio a_0/λ increases. For $a_0/\lambda = 0.2$, this value is about 15% greater than the one obtained for $a_0 = 0$ and $\lambda = L$.

Because of the variation of the thermal boundary-layer thickness as the radial distance becomes greater, the value of $\overline{Nu_P}\, Re_\omega^{-1/2}$ is evidently related to the number of cycles N which are encountered in the range $0 \leqslant r \leqslant L$. This influence appears in Fig. 4: the average Nusselt number is seen slowly increasing from $N = 1$ to 8. For $N > 8$ its value becomes constant.

Finally, it is noted in Fig. 5 that the influence of the ratio a_0/λ on the average heat transfer coefficient is also related to the nature of the fluid. In this figure, we have given $\overline{Nu_P}\, Re_\omega^{-1/2}$ against the Prandtl number for three values of a_0/λ. The roughness effects are seen to slowly increase with an increasing Prandtl number.

4. CALCULATION OF THE LOCAL WALL TEMPERATURE

In order to compare the theoretical results with experimental data, we must now deduce the wall temperatures from the heat flux condition (5). Because the experiments were performed with air in a relatively small enclosure (see the next section), we first assume that the radiation transmission factor of the fluid is unity. The heat flux q which appears in the boundary conditions (5) can thus be made explicit as

$$q = F_{12}\alpha_r Q\cos\beta - \varepsilon_r\sigma F_{2E}(T_w^4 - T_\infty^4) \quad (26)$$

where F_{12} is the view factor between a radiative heat source with density Q (subscript 1) and the sinusoidal area (subscript 2). F_{2E} is the view factor between the disk and all other surfaces which enclose the experimental apparatus. The surfaces are assumed to be at the fluid temperature far from the disk, T_∞.

We can write

$$F_{21} + F_{22} + F_{2E} = 1 \quad (27)$$

where F_{22} is the view factor between the different facing parts of the disk surface. We now assume that $F_{22} \ll F_{2E}$, which is in agreement with the low amplitude/wavelength ratio hypothesis. Moreover, the direction of incident heat source radiations is parallel to the axis of rotation, which is experimentally possible if the distance D between the source and the disk is relatively high in comparison with the radius L. We can thus write that $F_{21} \simeq 0$, so that equation (27) simplifies to $F_{2E} \simeq 1$. It should be noted that the configuration factor F_{12} depends on the position $x(\varepsilon)$. However, in accordance with the conditions $a_0/\lambda \ll 1$ and $L/D \ll 1$, F_{12} has been considered as a constant in the calculations.

The other quantities which appear in equation (26) are a_r and ε_r, the absorptivity and emissivity of the disk surface. (As the surface has been covered with black paint, then $a_r = \varepsilon_r$ for the infra-red wavelength range.) In addition σ is the Stefan–Boltzmann constant and β is the angle defined in Fig. 1.

With the above assumptions, the wall condition can be written as

$$-k\left.\frac{\partial T}{\partial y}\right|_{y=0} = q = F_{12}\alpha_r Q\cos\beta - \varepsilon_r\sigma(T_w^4 - T_\infty^4). \quad (28)$$

Figure 6 shows a typical wall temperature profile (curve 2) deduced from the thermal balance (28). Curve 1 represents the geometrical profile. For this example, the ratio a_0/λ is 0.2 which is the maximum value tested. The other quantities are $L = 0.03$ m, $\lambda = 0.01$ m and $Re_\omega = 250$. The figure shows the

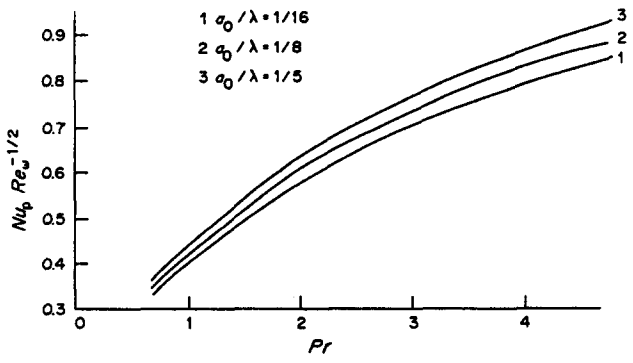

FIG. 5. Variation of the average Nusselt number $\overline{Nu_P}$ vs the Prandtl number for several values of the amplitude/wavelength ratio. $L = 0.03$ m, $\lambda = 0.01$ m.

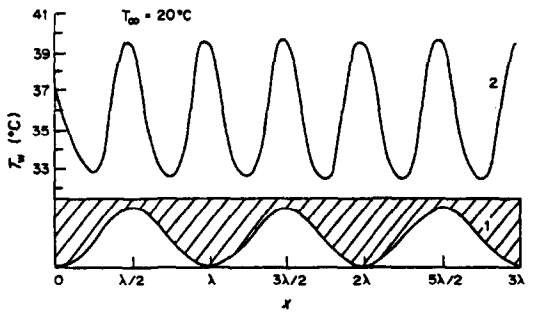

FIG. 6. Wall temperature profile vs the normal distance from the axis of rotation. $Pr = 0.7$, $L = 0.03$ m, $Re_\omega = 250$, $a_0/\lambda = 0.2$, $T_\infty = 20°C$, $Q = 78\,500$ W m^{-2}.

double periodicity of the temperature profile in comparison with the geometrical one. The minimum and maximum temperatures are obtained for the points which are located at $n\lambda/4$ and $n\lambda/2$, respectively (n is an integer). This appears to contradict the results shown in Fig. 3 where the maximum local Nusselt numbers are obtained for $n\lambda/2$. However, it should not be forgotten that the direction of the incident radiative heat flux is parallel to the axis of rotation so that the absorbed energy is greater for these points. We also note that the wall temperature at the axis of rotation is smaller than those which are obtained for the points located at $n\lambda/2$ (with $n \neq 0$), although the incident energy is the same. This is in agreement with Fig. 3, which shows that the convective heat transfer coefficient is higher at the axis.

Figure 7 shows the effect of the rotation velocity on the distribution of wall temperatures. The temperatures have been plotted against z for $a_0/\lambda = 1/6$. The cooling of the surface is better as the angular velocity increases and the profile amplitude is seen to decrease.

5. EXPERIMENTAL STUDY

5.1. *Experimental procedure*

The analysis of heat transfer from a rotating rough disk has been carried out using the experimental system shown in Fig. 8 [18, 19]. This apparatus has five components.

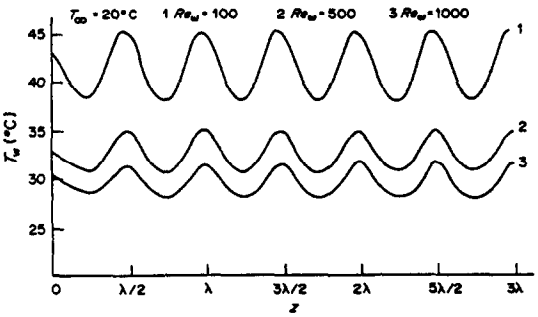

FIG. 7. Influence of the Reynolds number on the temperature profile. $Pr = 0.7$, $L = 0.03$ m, $a_0/\lambda = 0.167$, $T_\infty = 20°C$, $Q = 78\,500$ W m^{-2}.

(i) A thermographic infra-red camera (Inframetrics, model 525), the main specifications of which are:

temperature measurement range: −20°C to 1500°C
resolution of temperature measurements: 0.2°C
spectral range: 8–12 μm
detector: Hg Cd Te
detector coolant: liquid nitrogen.

(ii) A microcomputer for collection and treatment of data.

(iii) A cylindrical heater element with thermo-regulation. The infra-red camera is placed behind this hollow cylinder, the inner diameter and length of which are 7 and 10 cm, respectively.

(iv) An electric motor with chuck for the fixing and rotation of disks at a regulated angular speed. The disks rotate about a horizontal axis and their diameter is 6 cm. The disk material is 'nylon 6' and their surface is covered with black paint.

(v) A black body reference source.

Before collecting data, the preliminary control of heating uniformity on the surface of the disk and the verification of the steady state conditions are necessary.

In order to create a uniform radiant heat source for the disk, the axis of the heater and the axis of rotation are put in a line. Moreover, the distance between the heater and the disk is large (about 30 cm) compared to their diameter, so that the direction of the radiative heat flux can be considered parallel with the axis of rotation. The uniformity of the radiant heat source has been verified by observing the temperature of the surface for a rotating flat disk: according to theory and previous published experimental results, an isothermal surface was found.

Verification of steady state conditions was performed during each experiment by the process of data acquisition. A sequential data processor carried out the storage of thermal information (thermogram) at regular time steps (approximately 0.25 s). An example of a thermogram is shown in Fig. 9(a). The software allows the selection of a line from this thermogram and the corresponding thermal profile is calculated (Fig. 9(b)). Another function of the software computes a three-dimensional representation (256 lines × 256 columns × 64 levels) of temperature in relation to time. The steady state conditions are obtained when each successive thermal profile stays identical during acquisition (about 10 min).

Finally, it is important to remember that the theoretical study is based on the hypothesis of a ratio a_0/λ less than 0.2. This enables us to assume as a first approximation that the view factor between the concave surface of the sinusoid and surroundings is the same as the one between the convex surface of the sinusoid and surroundings. This hypothesis is even

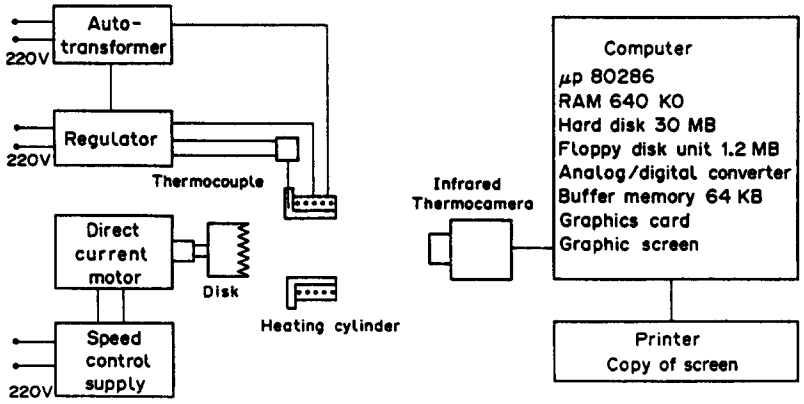

FIG. 8. System layout.

less valid when the ratio a_0/λ increases, as shown in Fig. 9, for which experiments were performed with $a_0/\lambda = 0.375$. Indeed, the view factor between the different facing parts of the surface (F_{22}) cannot be neglected and the cooling of the convex parts becomes more instense than the concave ones: there is a higher temperature for the troughs than for the peaks.

5.2. *Experimental results*

Figure 10 shows the qualitative results obtained for $a_0/\lambda = 0.125$. Measurements in the range $5\lambda/2 < r < 3\lambda$ have been omitted in this figure because they are highly affected by the edge effects.

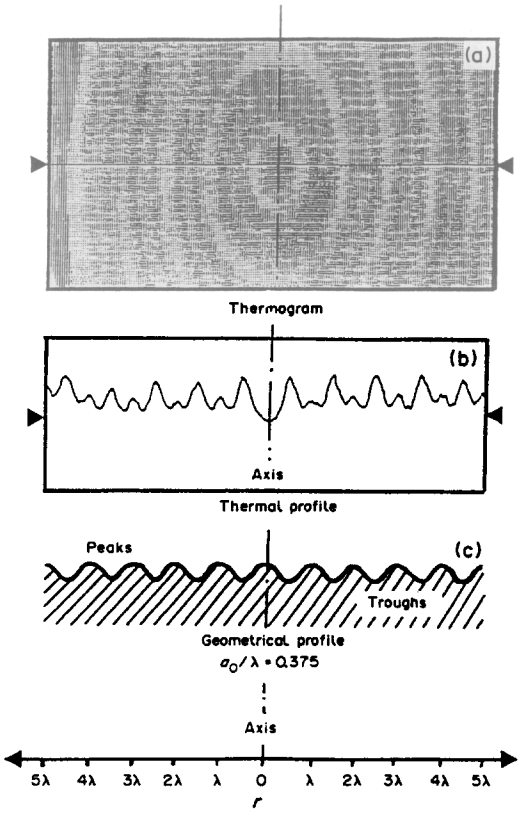

FIG. 9. Thermogram (a), thermal profile (b) and geometrical profile (c) for $a_0/\lambda > 0.2$ ($a_0/\lambda = 0.375$).

By comparing this figure with the thermal profile shown in Fig. 6, we note that the theoretical predictions agree with experimental observations: first of all, the periodicity of the thermal profile is doubled as compared with the geometrical one. Secondly, the temperature of peaks and troughs correspond to the maximum temperatures of the thermal profile and their values are identical on average. Lastly, we can see that the temperature of the middle peak is less significant than that of the other peaks, confirming the theoretical analysis developed in the preceding paragraphs.

In order to give some quantitative comparisons of results, we have shown in Fig. 11 the temperature range ΔT between the average maximum temperature (T_{max}) and the average minimum temperature of the thermal profile as a function of $(T_{max} - T_\infty)$. It should be noted that the temperature of the middle peak is omitted for the calculation of T_{max}, which can be varied by modifying either the incident flux or the rotation speed. We note a good agreement between the theoretical predictions (curve a) and experimental measurements for the values themselves, as well as for the slope of the straight line. The corresponding experimental profiles are given in Fig. 12: this series of experiments was carried out by modifying the intensity of the radiant heat source.

For the study of the rotating speed (the incident flux being fixed) the current system prevents us from showing the effects clearly, as the maximum rotational speed is 3000 revolutions per minute, which corresponds on average to a Richardson number of approximately 0.1 when the range $(T_w - T_\infty)$ is about 10°C. In this study, the Richardson number, Ri, is defined as

$$Ri = \frac{Gr}{Re_\omega^2} \tag{29}$$

where Gr is the Grashof number

$$Gr = \frac{g_0 \beta_T (T_w - T_\infty)\lambda^3}{\nu^2}. \tag{30}$$

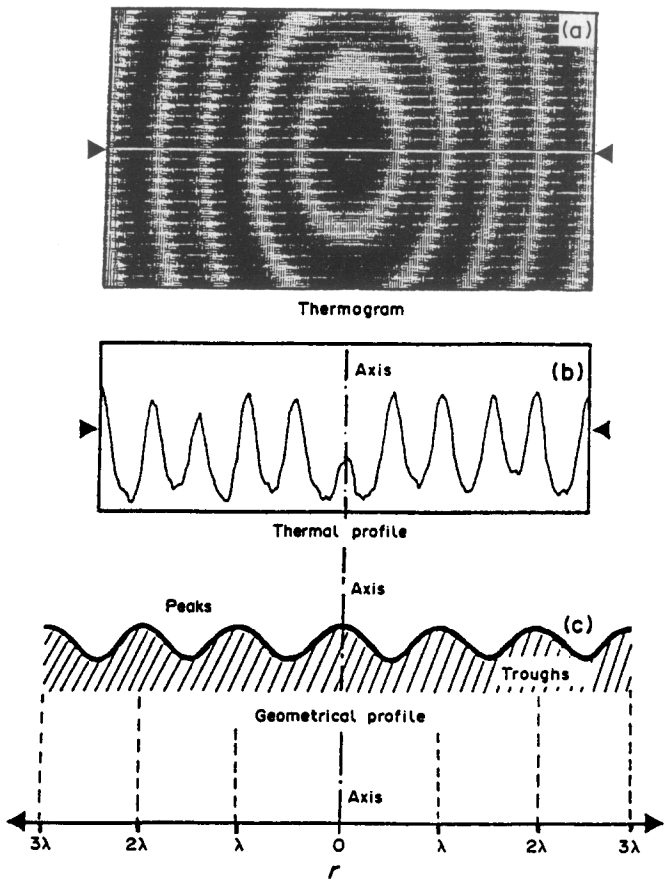

FIG. 10. Thermogram (a), thermal profile (b) and geometrical profile (c) for $a_0/\lambda = 0.125$.

According to a recent study [20], $Ri = 0.1$ is the limit above which the natural convection cannot be neglected for these types of flow. A speed less than 2000 revolutions per minute would therefore correspond to the mixed convection regime, which is not included in the context of this study.

6. CONCLUSIONS

We have presented a theoretical and experimental study of forced laminar convection, generated by the rotation of a disk, the surface of which is characterized by sinusoidal waves. The theoretical analysis, based on the boundary-layer equations, is justified both on qualitative and quantitative grounds by measurements of surface temperatures carried out by infrared thermography. The results exhibit the doubled periodicity of the thermal profile in comparison with the geometrical profile. They also illustrate the link existing between the increase of the Nusselt number and roughness. However, as explained above, this increase is also due to the oscillatory wall temperature of the rough disk.

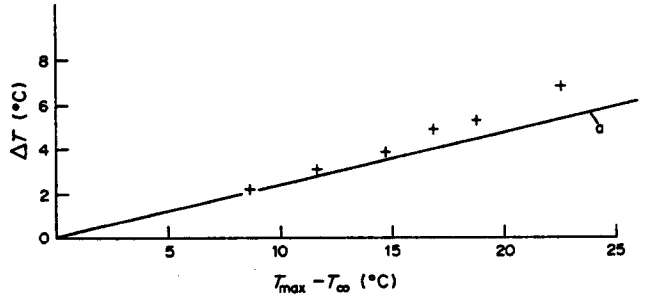

FIG. 11. Variation of ΔT as a function of $(T_{max} - T_\infty)$. Curve a, theory; +, experimental values.

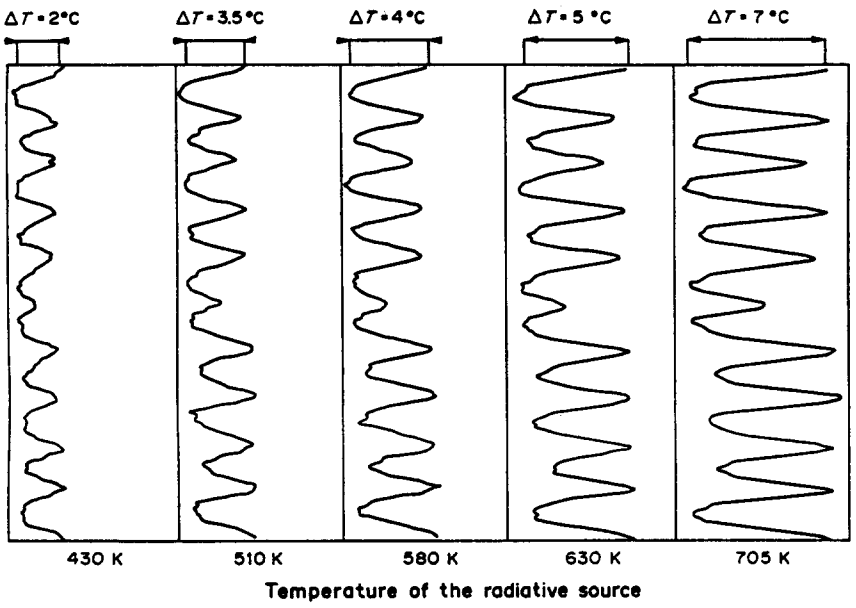

FIG. 12. Thermal profiles corresponding to the experimental values of Fig. 11.

REFERENCES

1. R. L. Webb, E. R. G. Eckert and R. J. Goldstein, Heat transfer and friction in tubes with repeated-rib roughness, *Int. J. Heat Mass Transfer* **14**, 601–617 (1971).
2. V. Gomelauri, Influence of two-dimensional artificial roughness on convective heat transfer, *Int. J. Heat Mass Transfer* **7**, 653–663 (1964).
3. D. F. Dipprey and R. H. Sabersky, Heat and momentum heat transfer in smooth and rough tubes at various Prandtl numbers, *Int. J. Heat Mass Transfer* **6**, 329–353 (1963).
4. D. Bettermann, Contribution à l'étude de la convection forcée turbulente le long de plaques rugueuses, *Int. J. Heat Mass Transfer* **9**, 153–164 (1966).
5. A. Singh, B. B. Mikic and W. M. Rohsenow, Active sites in boiling, *J. Heat Transfer* **98**, 401–406 (1976).
6. C. Saidi, F. Legay-Desesquelles and B. Prunet, Laminar flow past a sinusoidal cavity, *Int. J. Heat Mass Transfer* **30**, 649–661 (1987).
7. M. J. Strydom, Etude théorique de la convection forcée au-dessus d'une paroi sinusoidale en régime laminaire et permanent, Thesis, Perpignan (1985).
8. H. Abdurrachim, Etude théorique et expérimentale de la convection naturelle laminaire sur des surfaces ondulées, Thesis, Perpignan (1980).
9. E. M. Sparrow and J. L. Gregg, Heat transfer from a rotating disk to fluids of any Prandtl number, *Heat Transfer, Trans. ASME* **18**, 249–251 (1959).
10. L. A. Dorfman, *Hydrodynamic Resistance and Heat Loss of Rotating Solids*. Oliver & Boyd, Edinburgh (1963).
11. N. Riley, The heat transfer from a rotating disk, *Q. Mech. Appl. Math.* **17**, 331–349 (1964).
12. Narendra R. Vira and Dah-Nien Fan, Temperature distribution in generalized Von Karman rotating-disk flows, *Numer. Heat Transfer* **3**, 483–497 (1980).
13. H. B. Dwight, *Tables of Integrals and Other Mathematical Data* (4th Edn). Macmillan, Toronto (1969).
14. H. B. Keller and T. Cebeci, Accurate numerical methods for boundary-layer flows. Part I: two-dimensional laminar flows, Lecture Notes in Physics, 8, *Proc. Second Int. Conf. on Numerical Methods in Fluid Dynamics*, p. 92. Springer, New York (1971).
15. H. B. Keller and T. Cebeci, Accurate numerical methods for boundary-layer flows. Part II: two-dimensional turbulent flows, *AIAA J.* **10**, 1193–1199 (1972).
16. H. Görtler, A new series for the boundary-layer, *J. Math. Mech.* **16**, 1–66 (1957).
17. T. Cebeci and P. Bradshaw, *Momentum Transfer in Boundary Layers*. Hemisphere, Washington, DC (1977).
18. A. Nakayama, H. Koyama and S. Ohsawa, Theoretical and experimental study of turbulent separated flows behind a rotating axisymmetric body, *Numer. Heat Transfer* **7**, 359–371 (1984).
19. A. C. Roudot, M. Chuard, J. Mignot et D. Rondot, Mesure des températures locales de surface. Rôle de la microtopographie, *Rev. Phys. Appl.* **21**, 245–255 (1986).
20. G. Le Palec, A new correlation for laminar mixed convection over a rotating sphere, *Int. J. Heat Mass Transfer* **31**, 2347–2355 (1988).

ETUDE DU TRANSFERT DE CHALEUR LAMINAIRE SUR UN DISQUE TOURNANT AFFECTE D'ONDULATIONS SINUSOIDALES

Résumé—On étudie théoriquement et expérimentalement le transfert de chaleur laminaire sur un disque tournant affecté d'ondulations sinusoidales et soumis à un flux pariétal constant. La théorie est basée sur l'approximation de la couche limite. Les résultats mettent en évidence l'influence de la rugosité sur les nombres de Nusselt local et moyen. Les températures de surface sont obtenues à l'aide d'un bilan thermique à la paroi et sont comparées aux températures expérimentales mesurées, dans le cas de l'air, par thermographie infrarouge.

UNTERSUCHUNG DES LAMINAREN WÄRMEÜBERGANGS AN EINER SINUSFÖRMIGEN ROTIERENDEN SCHEIBE

Zusammenfassung—Eine theoretische und experimentelle Untersuchung der laminaren Konvektion an einer sinusförmigen rotierenden Scheibe mit konstanter Wärmestromdichte an der Oberfläche wird vorgestellt. Die Theorie basiert auf einem Grenzschichtansatz. Die Ergebnisse zeigen den Einfluß der Rauhigkeit auf die örtliche und mittlere Nusselt-Zahl. Die theoretisch ermittelten Wandtemperaturen werden aus einer einfachen Energiebilanz erhalten und mit den experimentell gemessenen Werten verglichen. Letztere werden für Luft ($Pr = 0{,}7$) mit Hilfe der Infrarot-Thermografie bestimmt.

ИССЛЕДОВАНИЕ ТЕПЛОПЕРЕНОСА ПРИ ЛАМИНАРНОМ ТЕЧЕНИИ НАД ВРАЩАЮЩИМСЯ ДИСКОМ СИНУСОИДАЛЬНОЙ ФОРМЫ

Аннотация—Теоретически и экспериментально исследуется Конвективный теплоперенос при ламинарном течении над вращающмся диском синусоидальной формы и постоянном тепловом потоке на стенке. Теория основана на приближении пограничного слоя. Результаты показывают влияние шероховатости на локальные и среднее значения числа Нуссельта. Температуры стенки теоретически рассчитываются на основе теплового баланса и сравниваются с экспериментальными данными, полученными методом инфракрасной термографии для воздуха ($Pr = 0{,}7$).